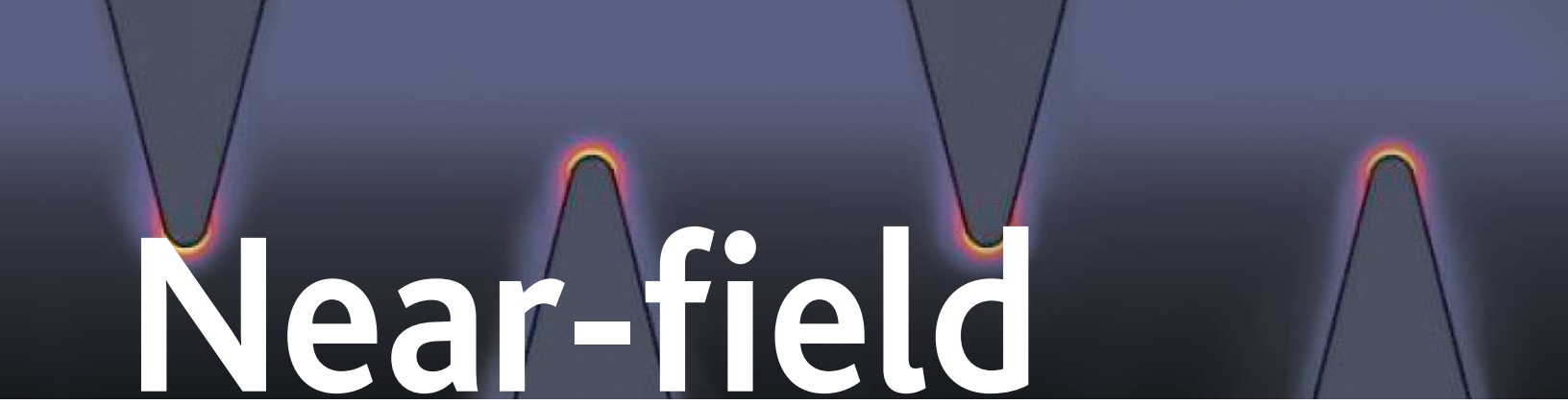

Near-field Raman microscopy

by Neil Anderson[†]*, Achim Hartschuh[‡], and Lukas Novotny[†]

Near-field microscopy offers the power of optical characterization with nanometer spatial resolution (~15 nm). Combining tip-enhanced microscopy with Raman scattering spectroscopy results in the ability to localize distinct spectral features, providing a unique opportunity to characterize materials on length scales of a few nanometers using visible light.

[†]Institute of Optics,
University of Rochester,
Rochester, NY 14627, USA
*E-mail: neanders@optics.rochester.edu

[‡]Physikalische Chemie,
Universität Siegen,
57068 Siegen, Germany

Near-field Raman microscopy has its origins in two distinct fields, namely near-field optics and Raman spectroscopy. The coming together of these two branches of science has seen the emergence of a powerful technique for characterizing materials with ultrahigh spatial resolution.

The origin of Raman spectroscopy dates back to the early 20th century. Theoretical predictions[1] postulated that photons should inelastically scatter from molecules in analogy to the Compton scattering of X-rays. In 1928, Raman and Krishnan[2] provided the first experimental evidence for such scattering events. Targeting a solution of chloroform with a beam of spectrally filtered sunlight, they detected the weak emission of yellow light. The origin of the yellow light is the Raman effect, in which the frequencies of the exciting light ω are mixed with the frequencies of molecular vibrations ω_n. This results in new frequencies $\omega \pm \omega_n$ similar to amplitude modulation in radio signal transmission.

With the invention of the laser, the last 40 years has witnessed the transformation of Raman spectroscopy into a sophisticated technique. However, it has only been in the last few years that conventional Raman scattering spectroscopy has been applied to the study of *localized* vibrational modes in nanoscale materials. Recent advances in imaging science[3,4] have enabled scientists to surpass the diffraction limit of classical optics and image subwavelength structures with spatial resolutions on the order of ~15 nm. One commonly used technique is tip-enhanced, near-field scanning optical microscopy (TE-NSOM), which makes use of the confined electric field at the apex of a sharp metal tip when placed in the focus of a strongly focused laser beam[5].

ISSN:1369 7021 © Elsevier Ltd 2005

Near-field optical microscopy can achieve spatial resolutions of a few nanometers and, by overcoming the limitations of conventional microscopy techniques, optical-based imaging and spectroscopy can be extended into the realm of quantum[6] and biological systems[7]. However, surpassing the resolution limits of optical microscopy is not confined to 21st century thinking. In the same year as Raman and Krishnan's pioneering work on the Raman effect, ideas on how to acquire subwavelength spatial resolutions were formulated by Synge[8]. He suggested that a quartz cone coated with a metal film, except for a small aperture at the cone apex, could be used as a nanoscale light source[9]. A breakthrough came with the development of subwavelength microwave microscopy by Ash and Nicholls[10], where image resolutions of $\lambda/23$ using 3 cm radiation were demonstrated. In 1984, two separate groups, led by Pohl[11] and Lewis[12], independently demonstrated that a subwavelength-sized aperture serving as a nanoscale light source could extend the technique into the visible spectrum. Using 488 nm radiation, Pohl and coworkers demonstrated spatial resolutions on the order of $\lambda/20$, compared with values of $\sim\lambda/2.5$ obtainable in conventional optical microscopy.

Over a decade later, the first experimental work in near-field Raman microscopy was reported. Hallen and coworkers[13], studying Rb-doped potassium titanyl phosphate ($KTiOPO_4$), demonstrated subwavelength Raman imaging within a spectral feature. Their early work showed the ability to map specific vibrational modes and produce corresponding topographic maps, something which far-field techniques cannot do. Following on from this work, Stöckle and coworkers[14] not only demonstrated high spatial resolutions on the order of 50 nm, but also the possibility of obtaining large enhancement factors. A metallized atomic force microscope (AFM) probe placed into the focus of a laser beam (on-axis illumination) and positioned within 10 nm of a thin cresyl blue layer resulted in Raman signals ~30 times larger than those recorded without the metallized tip. Using even sharper metal probes (with diameters of ~20 nm) to study C_{60} thin films, Stöckle *et al.* reported signals ~40 times greater than the Raman signal detected in the far-field. In comparing the far-field (~300 nm spot diameter) and near-field (~20 nm tip diameter) interaction volumes, the tip-induced Raman enhancement was estimated to be on the order of 10^4. Furthermore, tip-enhanced spectroscopic techniques have been used to locally induce coherent anti-Stokes Raman scattering (CARS) in biological species. Using metallized Si probes attached to an AFM-controlled cantilever, Kawata and coworkers[15] have visualized the structural network of adenine bases in DNA at a specific vibrational frequency (~1337 cm^{-1}) corresponding to the ring-breathing mode of the diazole in adenine.

Many near-field Raman schemes employ an on-axis illumination setup[5,13-15]. However, other illumination schemes can be employed to produce confined light sources and, thus, large enhancement effects (>10^2). Pettinger *et al.*[16] used a side-illumination scheme to study different molecular species absorbed on metallic surfaces, reporting enhancement factors on the order of 10^6. An alternative approach uses a scanning plasmon near-field optical microscope (SPNOM) combined with a standalone AFM. One such setup is based on a Kretschmann-Raether configuration, where a surface plasmon is excited at a Au-air interface and the probe is brought close to this interface. de Hollander and coworkers[17] used this technique to study metallic structures and report resolutions on the order of 20 nm. Surface plasmon resonances are strongly dependent on refractive index as well as surface roughness and sample thickness. Therefore, one advantage of using an SPNOM is the ability to study phase segregation with subwavelength resolution based on the different dielectric properties of spatially separate domains.

The ability to produce subwavelength Raman images is not solely dependent on producing highly confined electric fields at the apex of sharp metallic probes. Recent studies have demonstrated Raman imaging below the diffraction limit without field enhancement effects. Using uncoated fiber probes in a reflection geometry, Gucciardi and coworkers[18] achieved resolutions on the order of 100 nm operating at an excitation wavelength of 514.5 nm. This technique circumvents issues related to the production of highly confined light sources while still achieving spatial resolutions on the order of $\lambda/5$. However, the low throughput and signal-to-noise ratio of such fiber probes, coupled to the size of the aperture, limits the technique to the localization of vibrational modes with ~50 nm spatial resolution at best. To extend these Raman imaging capabilities below 10 nm, one needs either to use apertureless probes[5], where resolution is determined solely by the tip diameter, or to design new probe geometries based on current aperture probe techniques[19].

In this article, we focus on the use of sharp Au tips in an on-axis illumination scheme as a means to produce highly

confined fields. We illustrate the current state-of-the-art in Raman imaging and spectroscopy with examples taken from our own work on mapping vibrational modes along individual single-walled carbon nanotubes (SWNTs)[20,21].

Surface-enhanced Raman scattering

A Raman spectrum can be thought of as a unique fingerprint of the chemical composition and molecular structure of a material. However, the main drawback is that Raman scattering cross sections are several orders of magnitude (typically 10^{14} times) smaller than typical fluorescence cross sections. The discovery of signal enhancements on the order of 10^{14} in the presence of nanometer-sized metal structures (surface-enhanced Raman scattering, or SERS) allows the possibility of studying Raman scattering events at the single-molecule level[22]. It is widely accepted that the most significant contribution to the SERS effect is electromagnetic in origin and is caused by the enhancement of the local electric field E_{loc} with respect to the incident field E_i. The Raman enhancement factor M is defined as[23]:

$$M = [E_{loc}(\omega_i)/E_i(\omega_i)]^2 \times [E_{loc}(\omega_i-\omega_v)/E_i(\omega_i-\omega_v)]^2 \sim [E_{loc}(\omega_i)/E_i(\omega_i)]^4 \quad (1)$$

corresponding to the enhancement of both the incident field E_i at ω_i and the scattered field E_{loc} at ω_i-ω_v, where ω_i is the frequency of the incident field and ω_v is the vibrational mode frequency, respectively. In arriving at the last expression, we have taken $\omega_v << \omega_i$.

Field enhancement at a sharp metal tip

SERS has been used for many years as a way of enhancing weak Raman scattering signals[5,13-15,21,24-27]. The origin of the enhanced electromagnetic field is a combination of two distinct physical effects: the *lighting rod effect*, which is a result of the geometric singularity associated with sharply pointed metal structures; and *surface plasmon resonances*, which depend strongly on the excitation wavelength and are specific to the geometrical shape of a metal surface.

The key component of our tip-enhanced Raman imaging technique is the production of a confined electric field at a sharp Au tip. The field confinement is readily achieved if the polarization vector of the excitation light is orientated along the direction of the tip shaft. The result is a large buildup and confinement of an oscillating surface charge density at the tip apex (Fig. 1a)[26]. This electric field, localized to a volume of ~$(20\ nm)^3$, is used as our nanoscale Raman excitation source. The field-enhancement effect is much weaker if the exciting laser field is not polarized along the tip shaft (Fig. 1b). The maximum enhancement of the electric field intensity is $M = E_{loc}(r,\omega)^2/E_i(r,\omega)^2$.

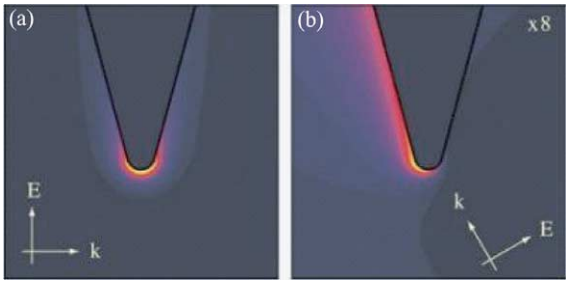

Fig. 1 Calculated field distribution at a sharp Au tip with a diameter of 5 nm. (a) Field distribution for an incident electric field vector parallel to the tip shaft showing localization of the electric field at the tip apex. (b) Field distribution for an incident electric field orientated nonparallel to the tip shaft. The field is no longer confined to the tip apex.

The sharp metal tips have two primary functions: to produce a highly confined electric field at the tip apex that acts as a nanoscale light source; and to propagate the high spatial frequency components of the Raman scattered light into the far-zone, i.e. the subwavelength information contained within the Raman scattered light. The influence of tip geometry and material is extremely important in producing strongly enhanced electric fields. We use high-purity Au wire that is electrochemically etched to an end radius of ~10-20 nm in a solution of HCl acid.

Experimental setup

We use a near-field Raman imaging system based on an inverted optical microscope fitted with an *x,y*-stage for raster-scanning samples (Fig. 2). A linearly polarized Gaussian mode from a continuous-wave He-Ne laser operating at 633 nm is used. Light from the laser is reflected using a dichroic beam splitter and focused onto the sample surface using a microscope objective with a high numerical aperture of 1.4. Having obtained a tight focal spot at the sample

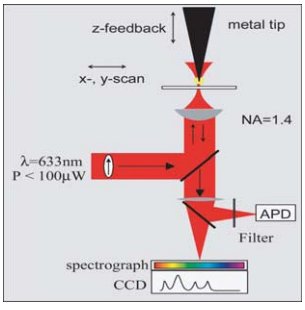

Fig. 2 Experimental arrangement for our on-axis illumination scheme.

surface, a sharp Au tip is placed into the focal region. The Au tip is mounted on one leg of a ceramic tuning fork (ν_{res} ~ 32 kHz) and held at a constant height of ~1-2 nm from the sample surface by means of a shear-force feedback mechanism[28]. Using the *x,y*-stage to raster scan our sample, Raman scattered light is collected using the microscope objective, transmitted by the same dichroic beam splitter, and detected using either a single-photon-counting avalanche photodiode (APD) or a spectrograph equipped with a charged-coupled device (CCD) cooled to -124°C. Acquisition times for recording a full Raman spectrum are on the order of a few hundred milliseconds. To produce the desired field enhancement in our on-axis illumination scheme (Fig. 2), the Au tip is displaced from the center of the focal region into one of the two longitudinal field lobes characteristic of a strongly focused Gaussian beam[5,15,21]. Alternatively, one may use a radially polarized mode, where the field lobe along the *z*-direction is located at the center of the focus and is typically several times stronger.

Tip-enhanced imaging and spectroscopy of SWNTs

SWNTs are the sample of choice for near-field Raman imaging and spectroscopy because they are truly one-dimensional nanoscale structures and have a well-defined Raman spectrum. The Raman scattering properties of SWNTs have been studied at length[29-31]. Kneipp *et al.*[32] studied the electromagnetic-enhancement effects of metal colloids on the Raman scattering of SWNTs and reported enhancement factors on the order of 10^{12}. Such high signal enhancements most likely originate from the intense electromagnetic fields found between small clusters of nanoscale metal particles.

The physical properties of nanotubes can be directly related to their physical dimensions. The ability to map local spectral features directly with spatial resolutions on the order of 15 nm allows us to attribute any spectral variations to structural changes and defects within the nanotube lattice[21].

The advantages of our technique, namely high spatial resolution and signal enhancement, are clearly demonstrated in Figs. 3 and 4, respectively. Fig. 3a shows the detected Raman scattered light (centered at 2600 cm^{-1}) for SWNTs dispersed on a glass cover slip. Fig. 3b is a scan of the same sample area with the inclusion of a sharp Au tip in the focus of the laser beam. We observe a sample containing a dispersion of individual and small bundles of SWNTs. The

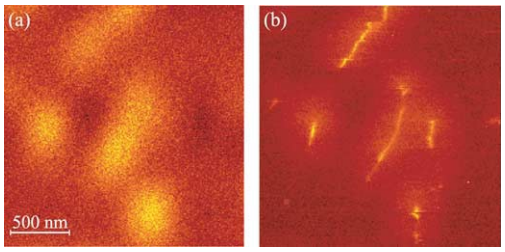

Fig. 3 Raman scattering images of SWNTs. (a) Confocal Raman scattering image integrated over the G' Raman band (~2600 cm^{-1}). (b) Raman scattering image taken over the same scan area with a sharp Au tip placed in the laser focus. The integration time per image pixel is ~10 ms (256 x 256 pixels).

lateral resolution (full width at half maximum) is 275 nm in Fig. 3a, i.e. ~λ/2.5, and 11 nm in Fig. 3b, i.e. ~λ/60. Fig. 4a shows a typical tip-enhanced Raman spectrum, showing the main Raman modes recorded for a specific location along an individual SWNT. Typical enhancement factors are on the order of 10^3-10^4. We recorded the Raman signal as a function of tip-sample distance to demonstrate the near-field nature of our technique (Fig. 4b). As is shown, the Raman signal rises significantly in the last few nanometers of the approach.

Having been able to apply our tip-enhanced near-field Raman technique to perform subwavelength microscopy, we now focus on using the technique to map the spatial variation of several Raman active bands along individual SWNTs. We record the spatial variation of the radial breathing mode (RBM) frequency (~100-300 cm^{-1}) and intensity of the disorder-induced D band (~1300 cm^{-1}) along an individual, spatially isolated SWNT. In addition, we also record the spatial variation of the intermediate frequency mode (IFM) (~600-1100 cm^{-1}) and the Raman-active G band (~1590 cm^{-1}) along the same nanotube.

Our work has addressed issues of nanotube uniformity and defect analysis at the single-nanotube level. Fig. 5 shows a

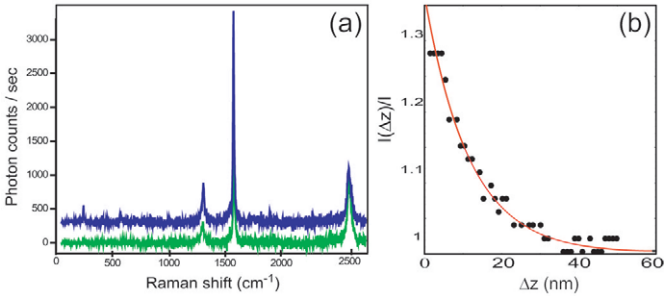

Fig. 4 Tip-enhanced Raman spectroscopy of an individual SWNT. (a) Tip-enhanced Raman scattering spectrum taken at a given location along an individual SWNT with and without a sharp Au tip present for an acquisition time of 210 ms. (Graphs offset for clarity). (b) Approach curve showing the distance dependence of the Raman intensity as the tip is positioned closer to the sample. (Part (b) reprinted with permission from[5]. © 2003 American Physical Society.)

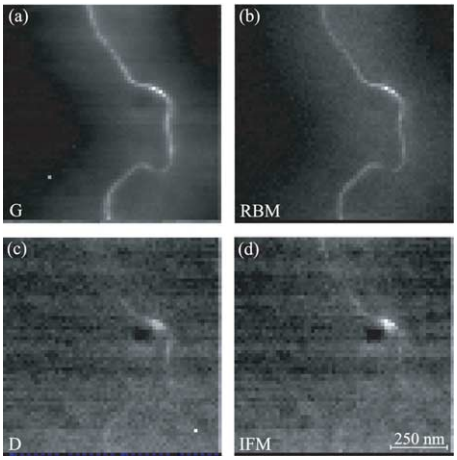

Fig. 5 Mapping vibrational modes along a CVD-grown SWNT: (a) G band (~1587 cm^{-1}); (b) RBM (~259 cm^{-1}); (c) D band (~1279 cm^{-1}); and (d) IFM (~835 cm^{-1}). The integration time per pixel is 210 ms (64 x 64 pixels).

series of near-field spectral images recorded along a SWNT grown by chemical vapor deposition: (a) G band; (b) RBM (259 cm^{-1}); (c) D band; and (d) IFM (835 cm^{-1}). From the spectral position of the RBM frequency, we determine the tube structure to be (n,m) = (8,5). The uniformity of the RBM frequency along the length of the SWNT indicates that the nanotube structure remains unchanged, even when the nanotube is resting on a supporting substrate (Fig. 5b). We observe a significant increase in Raman scattering intensity for the disorder-induced D band (Fig. 5c) and IFM (Fig. 5d) at the same location along the nanotube structure. However, both the G band (Fig. 5a) and RBM (Fig. 5b) signals are also enhanced at the same position, and this enhanced response may result from the close proximity of a large, 15 nm high particle, which is presumably residual iron(III) nitrate catalyst, indicated by a dark spot in Figs. 5a-d.

Outlook

Near-field Raman microscopy is a powerful tool for exploring physical properties of matter on length scales approaching those of semiconductor quantum structures and biological structures, such as individual proteins. Our recent work on mapping spatial variations of several Raman active modes for many different SWNTs has given new insights into nanotube uniformity and defect analysis on the single-nanotube level. Continued improvements in tip fabrication should enable much larger field enhancements and even higher spatial resolutions (<10 nm). A key challenge is the development and improvement of tip-based microscopy techniques to address fundamental questions on the physical properties of many biological systems. For example, the ability to interrogate single proteins inside a host membrane should provide a wealth of new information on physical properties and cellular function of such materials as never before. Finally, near-field Raman spectroscopy holds promise for probing subsurface defects and stress in nanoscale semiconductor structures. MT

Acknowledgments

The authors are grateful to Steve Cronin at Harvard University for providing CVD-grown SWNT samples. We would like to acknowledge financial support under MURI grant F-49620-03-0397 (Air Force Office for Scientific Research).

REFERENCES

1. Smekal, A., *Naturwissenschaften* (1923) **11**, 873
2. Raman, C. V., and Krishnan, K. S., *Nature* (1928) **121**, 501
3. Betzig, E., *et al.*, *Science* (1991) **251**, 1468
4. Betzig, E., and Chichester, R. J., *Science* (1993) **262**, 1422
5. Hartschuh, A., *et al.*, *Phys. Rev. Lett.* (2003) **90** (9), 095 503
6. Matsuda, K., *et al.*, *Phys. Rev. Lett.* (2003) **91** (17), 177 401
7. Xie, S. X., and Dunn, R. C., *Science* (1994) **265**, 361
8. Synge, E. H., *Philos. Mag.* (1928) **6**, 356
9. McMullan, D., The prehistory of scanned image microscopy. Part 1: Scanned optical microscopes, In *Selected Papers on Near-field Optics*, Jutamulia, S. (ed.), SPIE Milestone Series, (2002) **172**, 29 This text also serves as an excellent compilation of many important papers on near-field optics.
10. Ash, E., and Nicholls, G., *Nature* (1972) **237**, 510
11. Pohl, D. W., *et al.*, *Appl. Phys. Lett.* (1984) **44** (7), 651
12. Lewis, A., *et al.*, *Ultramicroscopy* (1984) **13** (3), 227
13. Jahncke, C. L. *et al.*, *Appl. Phys. Lett.* (1995) **67** (17), 2483
14. Stöckle, S. M., *et al.*, *Chem. Phys. Lett.* (2000) **318** (1-3), 131
15. Ichimura, T., *et al.*, *Phys. Rev. Lett.* (2004) **92** (22), 220 801
16. Pettinger, B., *et al.*, *Phys. Rev. Lett.* (2004) **92** (9), 096 101
17. de Hollander, R. G. B., *et al.*, *Ultramicroscopy* (1994) **57** (2-3), 263
18. Gucciardi, P. G., *et al.*, *Appl. Opt.* (2003) **42** (15), 2724
19. Frey, H. G., *et al.*, *Phys Rev. Lett.* (2004) **93** (20), 200 801
20. Hartschuh, A., *et al.*, *J. Microscopy* (2003) **210** (3), 234
21. Anderson, N., *et al.*, *J. Am. Chem. Soc.* (2005) **127** (8), 2533
22. Nie, S., and Emory, S. R., *Science* (1997) **275**, 1102
23. Kerker, M., *et al.*, *Appl. Opt.* (1980), **19** (19), 3373
24. Van Duyne, R. P., *et al.*, *J. Chem. Phys.* (1993) **99** (3), 2101
25. Novotny, L., *et al.*, *Phys. Rev. Lett.* (1997) **79** (4), 645
26. Wessel, J. E., *J. Opt. Soc. Am. B* (1985) **2** (9), 1538
27. Kawata, S., and Innouye, Y., *Ultramicroscopy* (1995) **57** (2-3), 313
28. Karrai, K., and Grober, R. D., *Appl. Phys. Lett.* (1995) **66** (14), 1842
29. Saito, R., *et al.*, *Physical Properties of Carbon Nanotubes*, Imperial College Press, London, (1998)
30. Jorio, A., *et al.*, *Phys. Rev. Lett.* (2001), **86** (6), 1118
31. Reich, S., *et al.*, *Carbon Nanotubes: Basic Concepts and Physical Properties*, Wiley-VCH, Cambridge, (2004)
32. Kneipp, K., *et al.*, *Phys. Rev. Lett.* (2000) **84** (15), 3470